electronics

MDPI

Article

Artificial Neural Network-Based Parameter Identification Method for Wireless Power Transfer Systems

Liangxi He [1], Sheng Zhao [1], Xiaoqiang Wang [2] and Chi-Kwan Lee [1,*]

1 Department of Electrical and Electronic Engineering, The University of Hong Kong, Hong Kong 999077, China; u3005900@connect.hku.hk (L.H.); shengz@hku.hk (S.Z.)
2 College of Electrical Engineering, Zhejiang University, Hangzhou 310058, China; xqwang0621@163.com
* Correspondence: cklee@eee.hku.hk

Abstract: In this paper, a Wireless Power Transfer (WPT) system parameter identification method that combines an artificial neural network and system modeling is presented. During wireless charging, there are two critical parameters; specifically, mutual inductance and load resistance, which change due to the movement of the transmitter/receiver and battery conditions. The identification of these two uncertain parameters is an essential prerequisite for the implementation of feedback control. The proposed method utilizes an Artificial Neural Network (ANN) to acquire a mutual inductance value. A succinct system model is formulated to calculate the load resistance of the remote receiver. The maximum error of the mutual inductance estimation is 2.93%, and the maximum error of the load resistance estimation is 7.4%. Compared to traditional methods, the proposed method provides an alternative way to obtain mutual inductance and load resistance using only primary-side information. Experimental results were provided to validate the effectiveness of the proposed method.

Keywords: artificial neural network; wireless power transfer; parameter identification

Citation: He, L.; Zhao, S.; Wang, X.; Lee, C.-K. Artificial Neural Network-Based Parameter Identification Method for Wireless Power Transfer Systems. *Electronics* **2022**, *11*, 1415. https://doi.org/10.3390/electronics11091415

Academic Editor: Domenico Mazzeo

Received: 1 April 2022
Accepted: 23 April 2022
Published: 28 April 2022

1. Introduction

Wireless power transfer (WPT) has drawn much attention in both the academic and industrial communities in recent years [1]. For example, WPT enables automated charging and eliminates shock hazards [2]. A WPT system employs a high-frequency alternating magnetic field to establish a transmission channel [3], allowing the energy to be cordlessly harnessed by the receiver. The basic constituent of a WPT system can be regarded as a resonant converter with a loosely coupled transformer [4–6]. WPT has the merits of safety, convenience, automation, and galvanic and mechanical isolation [7,8].

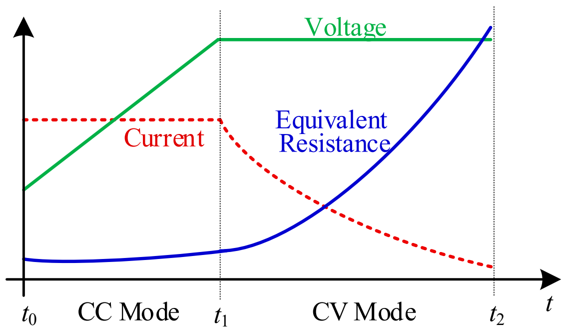

Figure 1. Typical CC-CV charging profile of a battery.

The mutual inductance in a WPT system varies as the vertical and horizontal receiver positions change. For example, when an electric vehicle is being wirelessly charged, the wireless charging transmitter mounted on the ground has a fixed position, but the receiver on the electric vehicle might not be coaxially aligned with the transmitter accurately, resulting in misalignment between the transmitter and the receiver [9]. Meanwhile, different types of vehicles, such as SUVs and sedans, vary in terms of height clearance; thus, the distance between the transmitter and receiver needs to be altered accordingly. Apart from the variations in mutual inductance, the equivalent load resistance should also be identified, as it is not a constant value during the dynamic charging process. Among the majority of WPT applications, batteries represent the most commonly used load type [10,11]. Battery charging consists of two stages: constant current (CC) followed by constant voltage (CV) charging [12–19], as illustrated in Figure 1. Therefore, the equivalent load resistance gradually increases according to the battery's state of charge (SOC) [20].

The control of a WPT system, such as the maximum power transfer or maximum energy efficiency [21–24], is reliant on the system parameters; hence, the mutual inductance and load value should be identified. Research has also been conducted regarding the identification of system parameters. In [25], a transient load detection model is presented for a voltage-fed WPT system using the energy injection mode and free resonant mode. In [26], a coupling coefficient estimation method is proposed that is based on the derivations of equations. However, the load value should be known in advance. Higher-order harmonics are regarded as information carriers that can be used to estimate the mutual inductance where one electrical signal and three circuit parameters are needed and can simplify the circuit [27]. In [28], the researchers propose a mutual inductance and load resistance identification technique at an operating frequency other than resonant frequency. In [29], load monitoring and power control is realized. This method converts an identification problem into an optimization problem, where the optimal solution achieves the minimum error. In [30], the authors use the rectifier load and equivalent inductance characteristics to determine the battery voltage and charging current, and equivalent load impedance is demonstrated. It is important to note that the identification parameters of an SS compensation network WPT system have been investigated in detail. Note that higher-order compensation network at WPT, i.e., LCC-LCC, is used extensively, but there is not adequate relevant research on this topic. Therefore, developing a method to bridge this research gap is needed, and LCC-LCC compensation network WPTs should also be considered. In this paper, an artificial neural network (ANN)-based technique is applied to estimate mutual the inductance of an LCC WPT system, and a system model is formulated to calculate the load resistance on the receiver side. ANNs have been reported to be a promising method for modeling electrical and electronic appliances [31]. In [32], ANNs were used in automatic impedance matching to maintain the power transfer efficiency. In this project, ANNs are used to predict the mutual inductance in the WPT system. Mutual inductance is first identified by measuring the horizontal and vertical distances, establishing a functional relationship between the mutual inductance and distance in the proposed ANN. As mutual inductance is not directly measurable, this method measures the distance, which substantially reduces the complexity of obtaining the mutual inductance. Subsequently, the load resistance is obtained via the formula derivation of the system model, in which only the input voltage and input current are needed to calculate the results.

This paper is organized as follows: Section 2 describes the WPT system model. Section 3 proposes the parameter identification technique based on the ANN. Section 4 presents the experimental results. Section 5 concludes this paper.

2. System Modelling

A representative schematic diagram of a WPT system with a double-sided LCC compensation topology is illustrated in Figure 2. Compared to the widely used S-S compensation topology, a double-sided LCC compensation topology has the advantages of coupling- and load-independent transmitter coil current characteristics, enabling better performance against the variations in mutual inductance and load resistance. On the primary side, a DC voltage source V_{in} is parallel to a capacitor C_{in} that is used to filter the harmonics and to provide constant voltage. The next segment is a full bridge inverter that can convert the

DC voltage to AC square voltage v_{ab}. This full bridge inverter consists of four switches (S_1–S_4). The resonant tank is constituted by L_a, C_a, C_p and L_p, whose resonant frequency is deliberately designed to have the same value as the switching frequency of the inverter. The resonant tank, which is formed by L_b, C_b, C_s and L_s on the secondary side, is also tuned to have the same resonant frequency as the primary-side resonant tank. A full bridge rectifier consists of four diodes (D_1–D_4). C_o is the output filter capacitor.

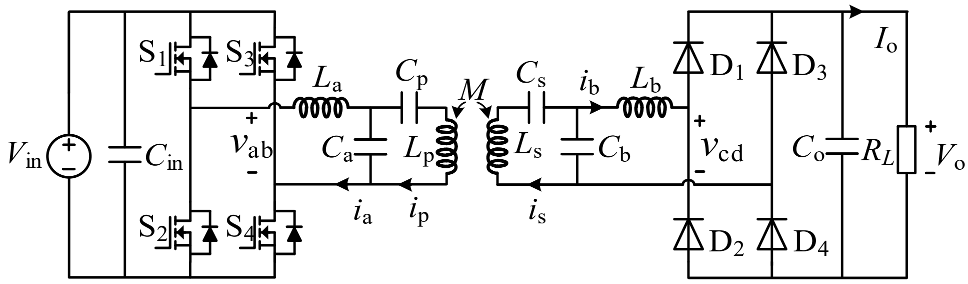

Figure 2. Schematic diagram of double-sided LCC WPT system.

In general, fundamental harmonic approximation (FHA) is utilized to simplify the analysis of the circuit while maintaining accuracy. The DC voltage and inverter portion can be replaced by an AC voltage source v_{ab}, and the rectifier together with the load resistance can be represented by an equivalent load R_e. A fundamental harmonic model can be established, as shown in Figure 3. The equivalent series resistance (ESR) is neglected.

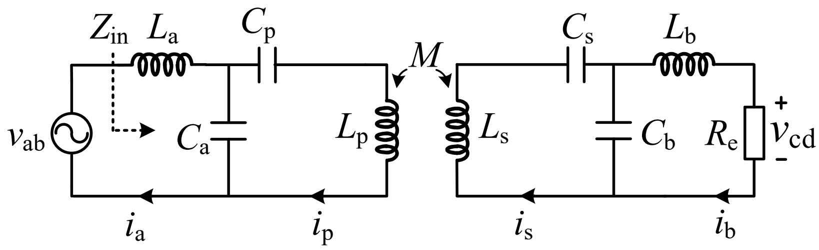

Figure 3. Fundamental harmonic model of double-sided LCC WPT system.

The compensation network obeys the following equation [33]:

$$\begin{cases} L_p - L_a = \frac{1}{\omega^2 \cdot C_p} \\ L_s - L_b = \frac{1}{\omega^2 \cdot C_s} \\ f = \frac{1}{2\pi\sqrt{L_a \cdot C_a}} = \frac{1}{2\pi\sqrt{L_b \cdot C_b}} \end{cases} \tag{1}$$

In this model, L_a resonates with C_a, and C_p resonates with the difference of what L_p subtracts L_a. Similarly, L_b resonates with C_b, and C_s resonates with the difference of what L_s subtracts L_b. According to Kirchhoff's voltage law (KVL), the WPT system can be described by the following matrix equation:

$$\begin{bmatrix} \dot{V}_{ab} \\ 0 \\ 0 \\ 0 \end{bmatrix} = \begin{bmatrix} Z_{11} & Z_{12} & 0 & 0 \\ Z_{21} & Z_{22} & Z_{23} & 0 \\ 0 & Z_{32} & Z_{33} & Z_{34} \\ 0 & 0 & Z_{43} & Z_{44} \end{bmatrix} \cdot \begin{bmatrix} \dot{I}_a \\ \dot{I}_p \\ \dot{I}_s \\ \dot{I}_b \end{bmatrix} \tag{2}$$

where $Z_{11} = j\omega L_a + \frac{1}{j\omega C_a}$, $Z_{12} = Z_{21} = -\frac{1}{j\omega C_a}$, $Z_{22} = j\omega L_p + \frac{1}{j\omega C_a} + \frac{1}{j\omega C_p}$, $Z_{23} = j\omega M$, $Z_{32} = -j\omega M$, $Z_{33} = j\omega L_s + \frac{1}{j\omega C_s} + \frac{1}{j\omega C_b}$, $Z_{34} = Z_{43} = -\frac{1}{j\omega C_b}$, $Z_{44} = j\omega L_b + \frac{1}{j\omega C_b} + R_e$.

On the secondary side, the equivalent impedance of L_s in series with C_s, which is represented by L_1, is an inductor that has the same value as L_b, which makes it a T-type LCL resonant circuit. The conversion from input voltage to the output current can be achieved by using this topology.

By applying KVL, we can obtain

$$\begin{bmatrix} \dot{V}_1 \\ 0 \end{bmatrix} = \begin{bmatrix} j\omega L_1 + \frac{1}{j\omega C_b} & -\frac{1}{j\omega C_b} \\ -\frac{1}{j\omega C_b} & j\omega L_b + \frac{1}{j\omega C_b} + R_e \end{bmatrix} \cdot \begin{bmatrix} \dot{I}_s \\ \dot{I}_b \end{bmatrix} \tag{3}$$

where V_1 is the equivalent voltage source on the receiver coil.

On the branch of the transmitter coil L_p on the primary side, there is a reflected impedance from the secondary side, and it satisfies

$$Z_{ref} = \frac{M^2 R_e}{L_b^2} \tag{4}$$

On the primary side, there is another LCL T-type resonant circuit, and therefore, the input impedance seen from the input voltage source v_{ab} is

$$Z_{in} = \frac{\omega^2 L_a^2}{Z_{ref}} \tag{5}$$

The current on the transmitter coil in phasor form is

$$\dot{I}_p = \frac{\dot{V}_{ab}}{j\omega L_a} \tag{6}$$

It can be observed from (6) the current is only decided by the input voltage v_{ab} and compensation inductance L_a, regardless of the mutual inductance M or load resistance R_e. Combining Equations (3) to (5) and assuming that $L_b = L_a$:

$$Z_{in} = \frac{\omega^2 L_a^4}{M^2 R_e} \tag{7}$$

Therefore, the equivalent AC load resistance can be obtained as

$$R_e = \frac{\omega^2 L_a^4}{M^2} \cdot \frac{I_a}{V_{ab}} \tag{8}$$

The equation above indicates that, once the input current and input voltage is known, the load resistance can be derived accordingly. The rest of this work uses the proposed artificial neural network to obtain the mutual inductance value.

3. Artificial Neural Network

In this section, ANN-based mutual inductance identification will be described to illustrate the mechanism of establishing the relationship between input and output.

For simplification, the vertical distance between the transmitter coil and receiver coil is defined as x, and the horizontal distance between the center of the transmitter coil and that of the receiver coil is defined as y, as illustrated in Figure 4. These two factors, x and y, are the input data, and the mutual inductance M is the output data. As a matter of fact, the mutual inductance M is only related to the relative position of the two coils, so the electrical parameters such as the input current and the input voltage are not taken into consideration. The flowchart of identification for both the mutual inductance and load resistance is shown in Figure 5. ANN has the potential to be trained to pick up hidden relationships that are difficult to find between the input and output. As mentioned previously, it is difficult to calculate the system parameters from the traditional analytical equations that model the relationship between the input–output properties. Therefore, an ANN is adopted to learn this relationship by training the model with data from the WPT system. In this situation, the input data are the vertical distance x and the horizontal distance y, and the output data are the mutual inductance M.

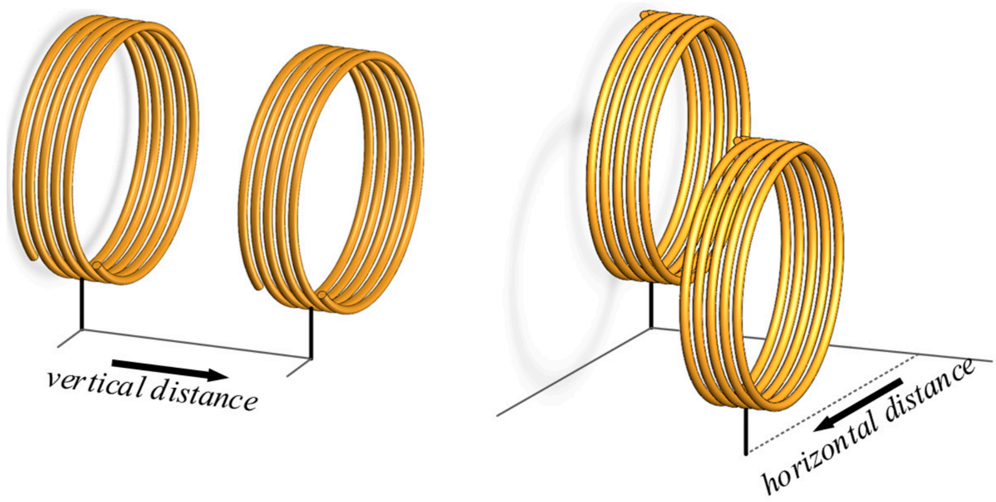

(**a**) (**b**)

Figure 4. Diagram of coil misalignments versus different (**a**) vertical distances and (**b**) horizontal distances.

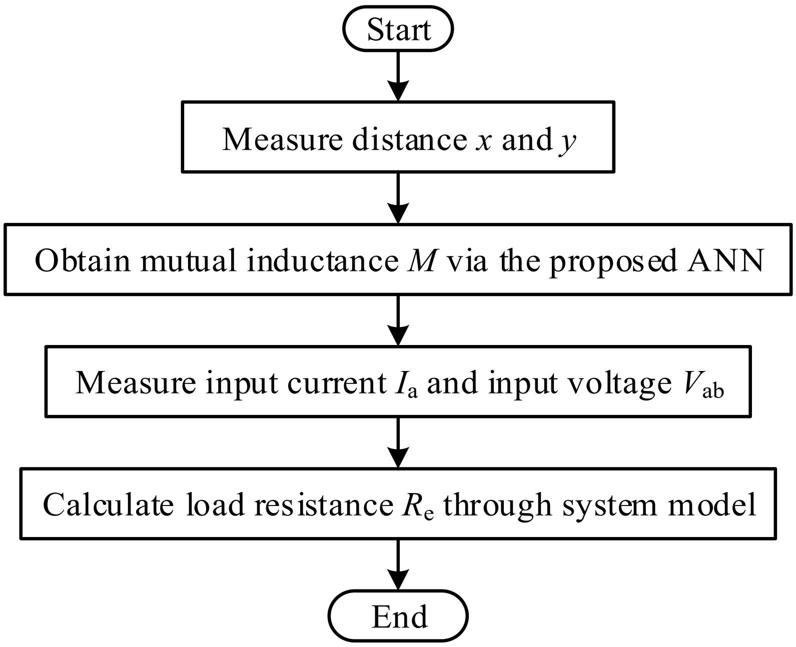

Figure 5. Flow chart of the identification process.

Figure 6 illustrates the basic structure of the ANN model [34,35] used for parameter identification in the WPT system [36]. ANNs are used to establish the architecture of the model using proper parameter selection. The artificial neural network represents the mapping between the input data and accurate output data. A widely used multi-layer perceptron (MLP) structure, which consists of an input layer, an output layer, and hidden layers, was adopted. The network architecture was adjusted according to its performance.

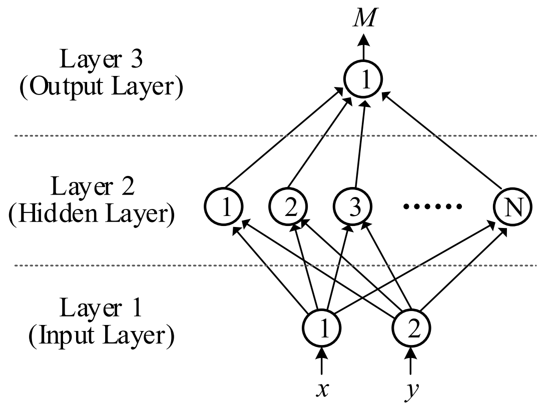

Figure 6. The structure of an ANN.

According to Figure 6, given the input vertical distance x and horizontal distance y, the output of the ANN model can be described as:

$$M = y_1 = \sum_{k=1}^{N} z_k w_{1k}^{(2)} + \eta \tag{9}$$

where η is the bias value for the output neurons, y_1 is the output value of the output neurons, N is the size of the hidden neurons, $w_{1k}^{(2)}$ is a weight parameter linking the neurons between the hidden layer and output layer, and z_k is the output value of the hidden neurons computed as:

$$\begin{cases} z_k = \sigma(\gamma_k) \\ \gamma_k = w_{1k}^{(1)} x + w_{2k}^{(1)} y + w_{0k}^{(1)} \end{cases} \tag{10}$$

where $\sigma(\cdot)$ is an activation function, $w_{1k}^{(1)}$ and $w_{2k}^{(1)}$ are the weight parameters linking the input neurons and the neurons in the hidden layer, and $w_{0k}^{(1)}$ is the bias value for the hidden neurons. This allows the input and output to be connected in a way that uses the sigmoid activation function of the neurons in the hidden layer.

$$\sigma(\gamma) = \frac{1}{1 + e^{-\gamma}} \tag{11}$$

Once the ANN architecture is determined, the next step is to develop an effective ANN model that can perform the prediction function. Therefore, it is of significance to input data to train this model. During the training process, the weight and bias data of the network will be adjusted until they reach their optimal values, minimizing the error between the measured and model-predicted M. In this project, the gradient-based quasi-Newton method is taken as the algorithm and has the ability to optimize the network simultaneously with good precision and speed. The index that reflects the accuracy of the ANN model is the relative error E_{ij}, which is defined as

$$E_{ij} = \frac{|y_{ij} - d_{ij}|}{d_{ij}} \tag{12}$$

where d_{ij} is the jth element of the measured data d_i, and y_{ij} is the jth element of the ANN model output y_i.

Data other than training data are used to verify the accuracy of the built ANN model. Equation (12) can be used to indicate the error between the predicted values of M and the measured M. With the help of the test error, it is easy to directly observe the effectiveness of the trained ANN model by judging if the error falls into an acceptable range. An ANN model is said to be acceptable if the error falls within a specific small range. Figure 7 provides a flowchart of the major steps for ANN training and testing.

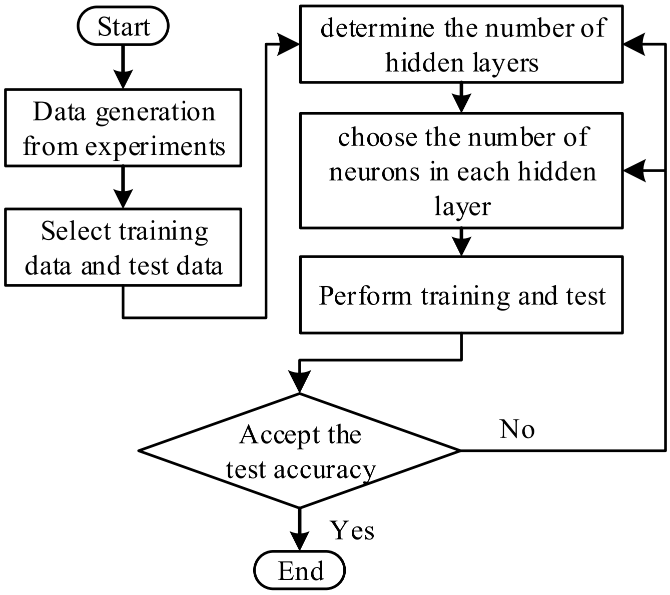

Figure 7. Flowchart of the steps for ANN training and testing.

After proper training and testing, it can be observed that when an ANN with a four-layer MLP structure consisting of an input layer, an output layer, and two hidden layers with fifteen neurons in the first hidden layer and ten neurons in the second hidden layer is adopted, the prediction of mutual inductance reaches a relatively acceptable level. Once mutual inductance identification is achieved by the ANN proposed above, the input current and input voltage will be measured by the sensors on the chip, and the load resistance will subsequently be calculated based on Equation (8).

4. Experimental Validation

In this section, the validity of the proposed identification method for mutual inductance and load resistance is verified using an experimental prototype. The schematic diagram is illustrated in Figure 8.

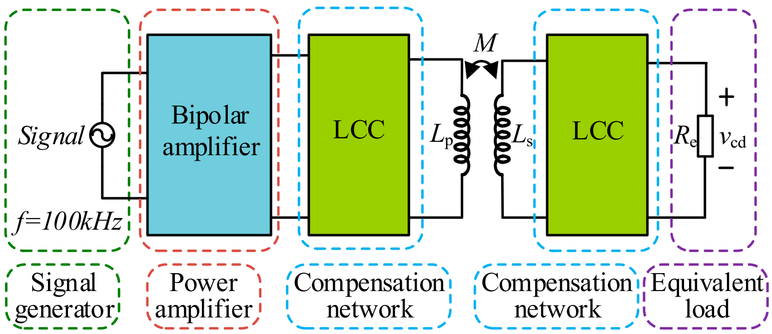

Figure 8. Schematic diagram of the experimental prototype.

4.1. Mutual Inductance

First of all, the mutual inductances with different distances are measured to provide training and testing data. First, the transmitter coil is perfectly coaxially aligned with the receiver coil, and their initial vertical distance is set to zero. Then, the receiver coil is moved in y direction by 5 mm once, and the mutual inductance is recorded until it reaches 100 mm. Afterwards, the receiver aligned coaxially aligned again, but the vertical distance is increased to 5 mm this time, and the y-direction movement mentioned above is repeated.

Additionally, the process is terminated when both the horizontal and vertical distances of the receiver reach 100 mm. Every x-direction pause contains 21 sets of y-direction data, and there are 21 sets of x-direction pauses. The 3-D plot of the measured mutual inductance is illustrated in Figure 9. It can be observed that, as the distance increases in either the x direction or y direction, the mutual inductance decreases monotonically.

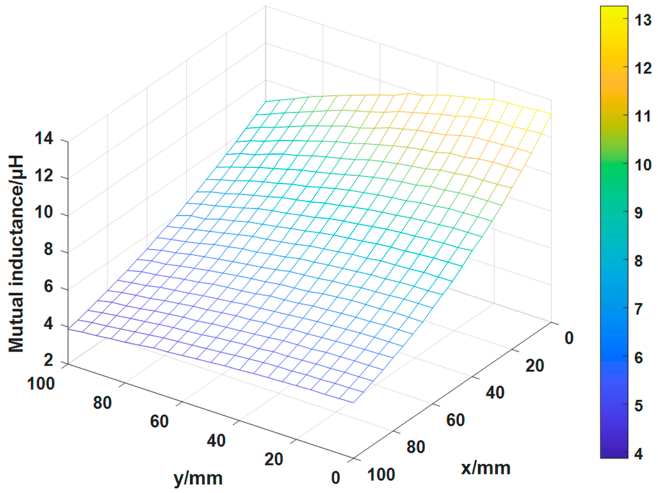

Figure 9. Measured mutual inductance with different x and y distances.

In the proposed artificial neural network model, the vertical distance x and the horizontal distance y are the input of the system, and the mutual inductance M is the output of the system. In order to investigate the influence of the training data on the prediction accuracy, three groups of experiments with different amounts of data were conducted.

Figure 10 shows the measured and predicted values of the results of the mutual inductance for the three training experiments, and only 10 x-direction sets are displayed. The blue curve represents the measured M, and the red dotted curve represents the corresponding ANN-calculated M. In the first training experiment, the first five x-direction sets of measured data are used as the training data. The remaining five sets of data are used to verify whether the model can predict the untrained data well. Next, with the trained model and five sets of untrained data, when x and y are used as inputs, the output of the trained model, numbered from 1 to 5 in Figure 10a, is compared to the corresponding measured data, and their relative errors are shown in the error bars. In the second training experiment, the first three sets of data are used as the training data. The remaining seven sets of data are used to verify whether the model can predict the untrained data well, as illustrated in Figure 10b. The last training experiment adopted the first two sets of data as the training data. The remaining eight sets of data are used to verify the model, as illustrated in Figure 10c. It can be seen that with the reduction in the training data, the misalignment between the blue curves and red dotted curves increases. Additionally, from the error bars, we can observe that the red dotted curves with smaller numbers show better alignment with the blue curves than those red dotted curves with bigger numbers, reflecting that the ANN model has better prediction ability for data that are more adjacent to the training data but that are relatively inadequate for use as remote data. Table 1 shows the corresponding errors for each experiment, including the maximum error and average error, which are within an admissible range. This verifies the effectiveness and robustness of the proposed ANN modeling method. More importantly, it is able to predict the mutual inductance with a large distance range accurately and only requires a small number of training samples.

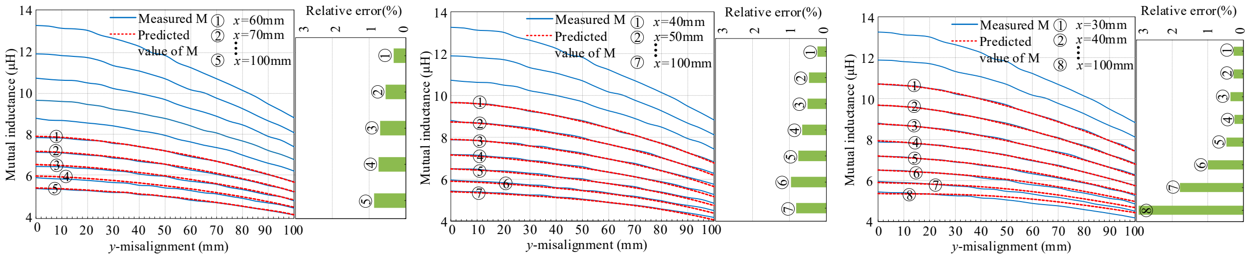

Figure 10. The consistency between the measured and predicted mutual inductance data based on the training data from (**a**) 5 sets; (**b**) 3 sets; (**c**) 2 sets.

Table 1. Error analysis of mutual inductance.

Error	Experiment 1	Experiment 2	Experiment 3
Maximum error	0.87%	0.96%	2.93%
Average error	0.64%	0.63%	0.91%

4.2. Load Calculation of WPT System

As stated in Section 2, the relationship between the load resistance and input voltage and current can be calculated from Equation (8). In this equation, all of the parameters with the exception of mutual inductance are constant and measurable, as listed in Table 2. Based on the analysis in part A, the mutual inductance can be estimated by the proposed artificial neural network, which makes all parameters in Equation (8) known. The estimated load resistance can then be calculated. To verify the effectiveness of the proposed method in terms of load resistance estimation, a WPT prototype was built that consists of a FeelTech FY2300 function generator, a HAS 4101 high-speed bipolar amplifier, an 11-turn series of transmitting and receiving coils made from Litz wire, LCC compensation networks on both sides, and resistors, as illustrated in Figure 11. Nine resistors with different values were used, and their actual values were compared to the calculated values according to Equation (8).

Table 2. System parameters of the WPT system.

Symbol	Parameter	Value
V_{ab}	Input AC voltage	10 V
f	Frequency	100 kHz
x	Vertical distance	0–100 mm
y	Horizontal distance	0–100 mm
L_a	Primary additional inductor	21.2 μH
C_a	Primary parallel capacitor	119.4 nF
C_p	Primary series capacitor	55.26 nF
L_p	Transmitter coil inductor	67.2 μH
L_s	Receiver coil inductor	67.2 μH
C_s	Secondary series capacitor	55.2 nF
C_b	Secondary parallel capacitor	120 nF
L_b	Secondary additional inductor	21.2 μH

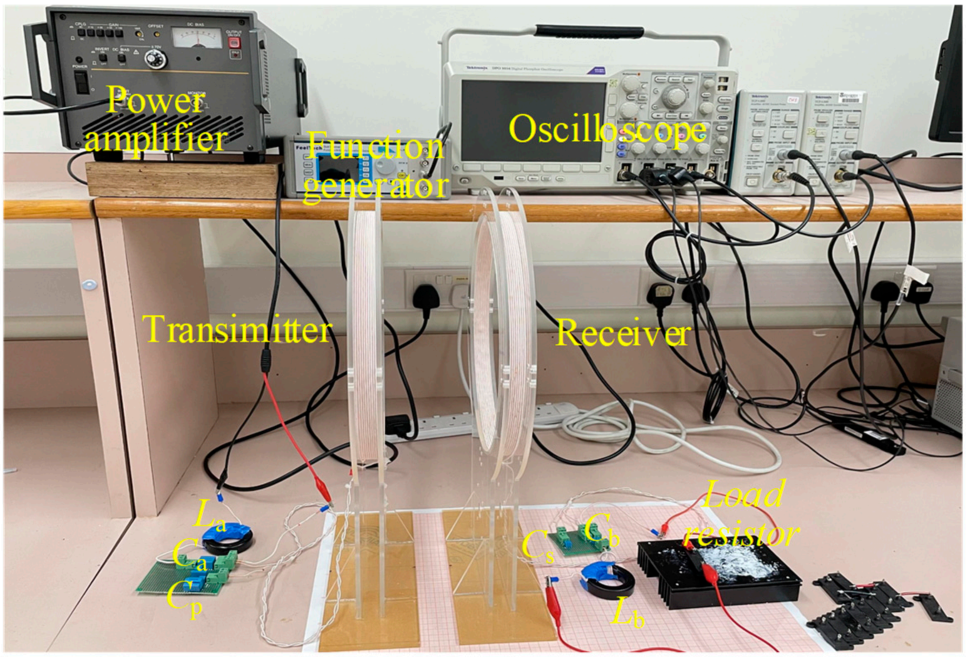

Figure 11. Experimental prototype.

As illustrated in Figure 12, the calculated load resistances are represented by blue marks, while the measured load resistances are represented by red marks. This experiment was conducted on the condition that the x distance was 0 mm, and the y distance was 0 mm. With the help of the proposed artificial neural network, it was easy to determine that the estimated mutual inductance was 13.26 µH. The measured load resistance values were 3.5 Ω, 4.4 Ω, 7.1 Ω, 12.5 Ω, 17.4 Ω, 24 Ω, 29.3 Ω, 34.5 Ω and 49.5 Ω, and the corresponding calculated load resistance values were 3.76 Ω, 4.64 Ω, 7.2 Ω, 12.54 Ω, 17.4 Ω, 23.97 Ω, 29.5 Ω, 34.6 Ω and 49.6 Ω. Figure 13 shows the rate error between the measured and calculated load resistance. It can be observed from Figure 13 that the estimated load resistances match the actual values well, and their relative errors were also analyzed, showing that the maximum error was 7.4% and the minimum error was 0.5%.

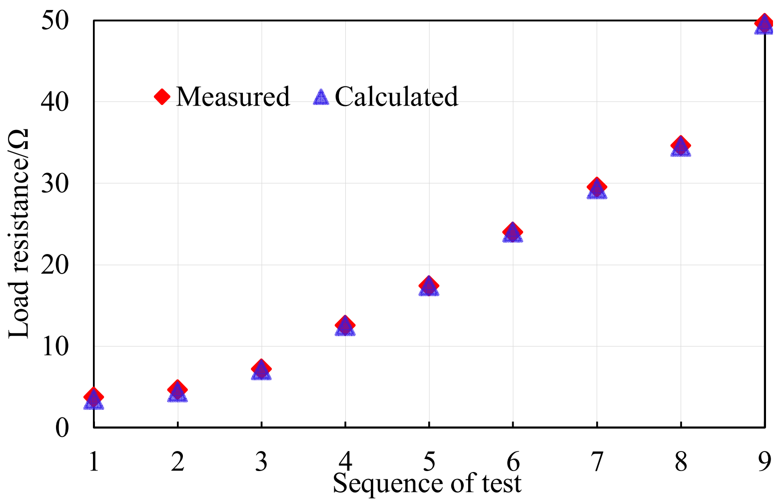

Figure 12. The consistency between the measured and calculated load resistance values.

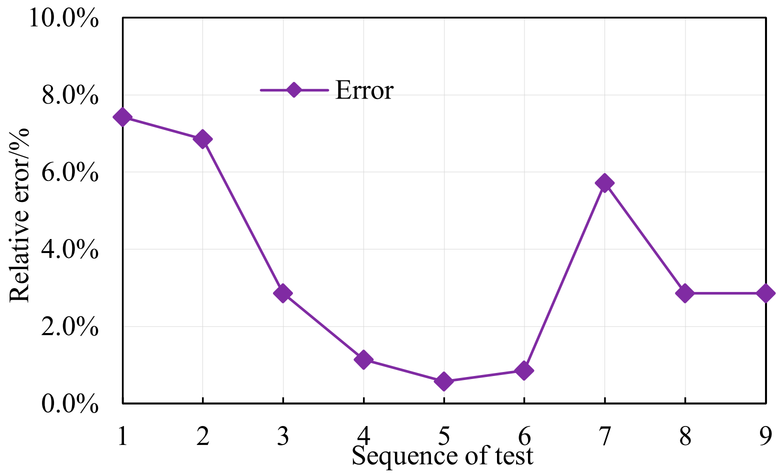

Figure 13. The error between the measured and calculated load resistance values.

5. Discussion

In this project, the mutual inductance values were measured and collected. Part of them were used as training data, and the rest were used as testing data. The proportion of training data to testing data varied from 5:5 to 3:7 and to 2:8 in order to observe the performance of the ANN model. The predicted mutual inductance values were found to be in better alignment with the testing data for mutual inductance when they were closer to the training data. Once the mutual inductance is determined, the load resistance can be subsequently calculated according to the predicted value. This finding provides a reference for control designs that aim to realize the constant current or constant voltage for charging batteries.

6. Conclusions

In this paper, a wireless power transfer system parameter identification method is proposed that is based on an artificial neural network and system model. The relationship between the vertical and horizontal misalignments and mutual inductance was determined by the artificial neural network, and equation derivation based on the LCC compensation networks reveals that the load resistance can be calculated according to input voltage, input current and estimated mutual inductance. The ANN simplified the calculation for mutual inductance by transforming the measuring targets. The effectiveness of the proposed method has been verified by experiments, where the maximum error of the mutual inductance estimation was determined to be 2.93%, and the maximum error of the load resistance estimation was 7.4%. The load resistance estimation errors are highly likely to be able to be produced by the noise from measuring equipment, and the calculated load resistance values fit well with the actual values. This study provides an alternative solution for parameter identification in WPT systems that only uses primary side information.

Author Contributions: Conceptualization, L.H.; methodology, S.Z.; supervision, C.-K.L.; visualization, X.W. All authors have read and agreed to the published version of the manuscript.

Funding: This research was funded by Hong Kong Research Grant Council under the General Research Fund Projects, grant number 17210420 and Theme-based Research Scheme (T23-701/20-R).

Institutional Review Board Statement: Not applicable.

Informed Consent Statement: Not applicable.

Data Availability Statement: Not applicable.

Conflicts of Interest: The authors declare no conflict of interest.

Nomenclature

V_{in}	DC input voltage
v_1	Equivalent voltage source on the secondary side
C_{in}	Input capacitor
S_i	ith MOSFET in the inverter
D_i	ith diode in the rectifier
L_{p}	Transmitter coil
L_{a}	Primary additional inductor
C_{a}	Primary parallel capacitor
C_{p}	Primary series capacitor
L_{s}	Receiver coil
L_{b}	Secondary additional inductor
C_{s}	Secondary series capacitor
C_{b}	Secondary parallel capacitor
C_{o}	Output filter capacitor
R_{L}	Load resistance
v_{ab}	AC voltage at the output of inverter
i_{a}	Current through the primary additional inductor
i_{p}	Current through the transmitter coil
M	Mutual inductance between transmitter coil and receiver coil
i_{s}	Current through the receiver coil
i_{b}	Current through the secondary additional inductor
v_{cd}	AC voltage at the input of rectifier
I_{o}	Current through the load
Z_{in}	Input impedance at the inverter output
Z_{ref}	Reflected impedance
ω	Resonant angular frequency
R_{e}	Equivalent load resistance

References

1. Zhang, Z.; Pang, H.; Georgiadis, A.; Cecati, C. Wireless Power Transfer—An Overview. *IEEE Trans. Ind. Electron.* **2019**, *66*, 1044–1058. [CrossRef]
2. Ahmad, A.; Alam, M.S.; Chabaan, R. A Comprehensive Review of Wireless Charging Technologies for Electric Vehicles. *IEEE Trans. Transp. Electrif.* **2018**, *4*, 38–63. [CrossRef]
3. Beh, H.Z.; Neath, M.; Boys, J.T.; Covic, G.A. An Alternative IPT Pickup Controller for Material Handling Using a Current Doubler. *IEEE Trans. Power Electron.* **2018**, *33*, 10135–10147. [CrossRef]
4. Vu, V.; Tran, D.; Choi, W. Implementation of the Constant Current and Constant Voltage Charge of Inductive Power Transfer Systems with the Double-Sided LCC Compensation Topology for Electric Vehicle Battery Charge Applications. *IEEE Trans. Power Electron.* **2018**, *33*, 7398–7410. [CrossRef]
5. Zhang, W.; White, J.C.; Abraham, A.M.; Mi, C.C. Loosely Coupled Transformer Structure and Interoperability Study for EV Wireless Charging Systems. *IEEE Trans. Power Electron.* **2015**, *30*, 6356–6367. [CrossRef]
6. Hou, J.; Chen, Q.; Zhang, Z.; Wong, S.-C.; Tse, C.K. Analysis of Output Current Characteristics for Higher Order Primary Compensation in Inductive Power Transfer Systems. *IEEE Trans. Power Electron.* **2018**, *33*, 6807–6821. [CrossRef]
7. Huang, Z.; Wong, S.; Tse, C.K. Design of a Single-Stage Inductive-Power-Transfer Converter for Efficient EV Battery Charging. *IEEE Trans. Veh.* **2017**, *66*, 5808–5821. [CrossRef]
8. Wang, X.; Xu, J.; Leng, M.; Ma, H.; He, S. A Hybrid Control Strategy of LCC-S Compensated WPT System for Wide Output Voltage and ZVS Range with Minimized Reactive Current. *IEEE Trans. Ind. Electron.* **2021**, *68*, 7908–7920. [CrossRef]
9. Chow, J.P.; Chung, H.S.; Cheng, C. Use of Transmitter-Side Electrical Information to Estimate Mutual Inductance and Regulate Receiver-Side Power in Wireless Inductive Link. *IEEE Trans. Power Electron.* **2016**, *31*, 6079–6091. [CrossRef]
10. Zhong, W.; Hui, S.Y. Reconfigurable Wireless Power Transfer Systems with High Energy Efficiency over Wide Load Range. *IEEE Trans. Power Electron.* **2018**, *33*, 6379–6390. [CrossRef]
11. Wang, Y.; Shi, G.; Yao, Y.; Alonso, J.M.; Weifeng, G.; Liu, X.; Xu, D. A Double-T-Type Compensation Network and Its Tuning Method for IPT System. *IEEE Trans. Ind. Electron.* **2017**, *53*, 4757–4767. [CrossRef]
12. Liu, F.; Chen, K.; Zhao, Z.; Li, K.; Yuan, L. Transmitter-Side Control of Both the CC and CV Modes for the Wireless EV Charging System with the Weak Communication. *IEEE Trans. Emerg. Sel.* **2018**, *6*, 955–965. [CrossRef]
13. Darvish, P.; Mekhilef, S.; Illias, H.A.B. A Novel S–S–LCLCC Compensation for Three-Coil WPT to Improve Misalignment and Energy Efficiency Stiffness of Wireless Charging System. *IEEE Trans. Power Electron.* **2021**, *36*, 1341–1355. [CrossRef]

14. Yue, R.; Wang, C.; Li, H.; Liu, Y. Constant-Voltage and Constant-Current Output Using P-CLCL Compensation Circuit for Single-Switch Inductive Power Transfer. *IEEE Trans. Power Electron.* **2021**, *36*, 5181–5190. [CrossRef]
15. Song, K.; Li, Z.; Jiang, J.; Zhu, C. Constant Current/Voltage Charging Operation for Series–Series and Series–Parallel Compensated Wireless Power Transfer Systems Employing Primary-Side Controller. *IEEE Trans. Power Electron.* **2018**, *33*, 8065–8080. [CrossRef]
16. Li, Z.; Liu, H.; Tian, Y.; Liu, Y. Constant Current/Voltage Charging for Primary-Side Controlled Wireless Charging System Without Using Dual-Side Communication. *IEEE Trans. Power Electron.* **2021**, *36*, 13562–13577. [CrossRef]
17. Li, Y.; Hu, J.; Li, X.; Chen, F.; Xu, Q.; Mai, R.; He, Z. Analysis, Design, and Experimental Verification of a Mixed High-Order Compensations-Based WPT System with Constant Current Outputs for Driving Multistring LEDs. *IEEE Trans. Ind. Electron.* **2020**, *67*, 203–213. [CrossRef]
18. Kavimandan, U.D.; Mahajan, S.M.; van Neste, C.W. Analysis and Demonstration of a Dynamic ZVS Angle Control Using a Tuning Capacitor in a Wireless Power Transfer System. *IEEE Trans. Emerg. Sel.* **2021**, *9*, 1876–1890. [CrossRef]
19. Huang, Z.; Wong, S.; Tse, C.K. An Inductive-Power-Transfer Converter with High Efficiency Throughout Battery-Charging Process. *IEEE Trans. Power Electron.* **2019**, *34*, 10245–10255. [CrossRef]
20. Guo, Y.; Zhang, Y.; Zhang, W.; Wang, L. Battery Parameter Identification Based on Wireless Power Transfer System with Rectifier Load. *IEEE Trans. Ind. Electron.* **2021**, *68*, 6893–6904. [CrossRef]
21. Hui, S.Y.R.; Zhong, W.; Lee, C.K. A Critical Review of Recent Progress in Mid-Range Wireless Power Transfer. *IEEE Trans. Power Electron.* **2014**, *29*, 4500–4511. [CrossRef]
22. Zhong, W.X.; Hui, S.Y.R. Maximum Energy Efficiency Tracking for Wireless Power Transfer Systems. *IEEE Trans. Power Electron.* **2015**, *30*, 4025–4034. [CrossRef]
23. Tang, X.; Zeng, J.; Pun, K.P.; Mai, S.; Zhang, C.; Wang, Z. Low-Cost Maximum Efficiency Tracking Method for Wireless Power Transfer Systems. *IEEE Trans. Power Electron.* **2018**, *33*, 5317–5329. [CrossRef]
24. Wang, X.; Xu, J.; Ma, H.; He, S. Inductive Power Transfer Systems with Digital Switch-Controlled Capacitor for Maximum Efficiency Point Tracking. *IEEE Trans. Ind. Electron.* **2021**, *68*, 9467–9480. [CrossRef]
25. Wang, Z.; Li, Y.; Sun, Y.; Tang, C.; Lv, X. Load Detection Model of Voltage-Fed Inductive Power Transfer System. *IEEE Trans. Power Electron.* **2013**, *28*, 5233–5243. [CrossRef]
26. Jiwariyavej, V.; Imura, T.; Hori, Y. Coupling Coefficients Estimation of Wireless Power Transfer System via Magnetic Resonance Coupling Using Information from Either Side of the System. *IEEE Trans. Emerg. Sel.* **2015**, *3*, 191–200. [CrossRef]
27. Hu, J.; Zhao, J.; Cui, C. A Wide Charging Range Wireless Power Transfer Control System with Harmonic Current to Estimate the Coupling Coefficient. *IEEE Trans. Power Electron.* **2021**, *36*, 5082–5094. [CrossRef]
28. Yin, J.; Lin, D.; Parisini, T.; Hui, S.Y. Front-End Monitoring of the Mutual Inductance and Load Resistance in a Series–Series Compensated Wireless Power Transfer System. *IEEE Trans. Power Electron.* **2016**, *31*, 7339–7352. [CrossRef]
29. Yin, J.; Lin, D.; Lee, C.; Hui, S.Y.R. A Systematic Approach for Load Monitoring and Power Control in Wireless Power Transfer Systems without Any Direct Output Measurement. *IEEE Trans. Power Electron.* **2015**, *30*, 1657–1667. [CrossRef]
30. Guo, Y.; Zhang, Y. Secondary Side Voltage and Current Estimation of Wireless Power Transfer Systems. *IEEE Trans. Ind. Appl.* **2022**, *58*, 1222–1230. [CrossRef]
31. Roshani, S.; Jamshidi, M.B.; Mohebi, F.; Roshani, S. Design and Modeling of a Compact Power Divider with Squared Resonators Using Artificial Intelligence. *Wireless Pers Commun.* **2021**, *117*, 2085–2096. [CrossRef]
32. Li, Y.; Dong, W.; Yang, Q.; Zhao, J.; Liu, L.; Feng, S. An Automatic Impedance Matching Method Based on the Feedforward-Backpropagation Neural Network for a WPT System. *IEEE Trans. Ind. Electron.* **2019**, *66*, 3963–3972. [CrossRef]
33. Fu, N.; Deng, J.; Wang, Z.; Wang, W.; Wang, S. A Hybrid Mode Control Strategy for LCC–LCC- Compensated WPT System with Wide ZVS Operation. *IEEE Trans. Power Electron.* **2022**, *37*, 2449–2460. [CrossRef]
34. Villegas-Mier, C.; Rodriguez-Resendiz, J.; Álvarez-Alvarado, J.M.; Rodriguez-Resendiz, H.; Herrera-Navarro, A.; Rodríguez-Abreo, O. Artificial neural networks in MPPT algorithms for optimization of photovoltaic power systems: A review. *Micromachines* **2021**, *12*, 1260. [CrossRef]
35. Rodríguez-Abreo, O.; Rodríguez-Reséndiz, J.; Fuentes-Silva, C.; Hernández-Alvarado, R.; Falcón, M.D.C.P.T. Self-Tuning Neural Network PID with Dynamic Response Control. *IEEE Access* **2021**, *9*, 65206–65215. [CrossRef]
36. Zhao, S.; Fu, H. An artificial neural network-based approach for the impedance modeling of piezoelectric energy harvesting devices. *Int. J. Numer. Model. Electron. Netw. Devices Fields* **2018**, *31*, 2333. [CrossRef]